Basin-scale estimates of greenhouse gas emissions from the Mara River, Kenya: Importance of discharge, stream size, and land use/land cover

Ricky M. Mwanake [1], Gretchen M. Gettel [1,2]*, Clarisse Ishimwe,[2] Elizabeth G. Wangari [1], Klaus Butterbach-Bahl [1,3], Ralf Kiese [1]

[1]Karlsruhe Institute of Technology, Institute for Meteorology and Climate Research, Atmospheric Environmental Research (IMK-IFU), Garmisch-Partenkirchen, Germany
[2]IHE Delft Institute for Water Education, Delft
[3]Mazingira Centre, International Livestock Research Institute (ILRI), Nairobi, Kenya

Abstract

Greenhouse gas fluxes (CO_2, CH_4, and N_2O) from African streams and rivers are under-represented in global datasets, resulting in uncertainties in their contributions to regional and global budgets. We conducted year-long sampling of 59 sites in a nested-catchment design in the Mara River, Kenya in which fluxes were quantified and their underlying controls assessed. We estimated annual basin-scale greenhouse gas emissions from measured in-stream gas concentrations, modeled gas transfer velocities, and determined the sensitivity of up-scaling to discharge. Based on the total annual CO_2-equivalent emissions calculated from global warming potentials (GWP), the Mara basin was a net greenhouse gas source (294 ± 35 Gg CO_2 eq yr^{-1}). Lower-order streams (1–3) contributed 81% of the total fluxes, and higher stream orders (4–8) contributed 19%. Cropland-draining streams also exhibited higher fluxes compared to forested streams. Seasonality in stream discharge affected stream widths (and stream area) and gas exchange rates, strongly influencing the basin-wide annual flux, which was 10 times higher during the high and medium discharge periods than the low discharge period. The basin-wide estimate was underestimated by up to 36% if discharge was ignored, and up to 37% for lower stream orders. Future research should therefore include seasonality in stream surface areas in upscaling procedures to better constrain basin-wide fluxes. Given that agricultural activities are a major factor increasing riverine greenhouse gas fluxes in the study region, increased conversion of forests and agricultural intensification has the possibility of increasing the contribution of the African continent to global greenhouse gas sources.

Inland waters emit ~ 20% (4.3 Pg-C yr^{-1}) of the global carbon budget to the atmosphere (Drake et al. 2018; Rosentreter et al. 2021), with tropical ecosystems in the Amazon and in Africa contributing 40% of these emissions (0.95 Pg-C yr^{-1} and 0.9 Pg-CH_4 yr^{-1}, respectively; Sawakuchi et al. 2017; Borges et al. 2015). Inland waters also contribute significantly to global N_2O emissions (Hu et al. 2016; Marzadri et al. 2021), with tropical rivers contributing ~ 2 Gg N_2O-N yr^{-1} (Yao et al. 2020). The African river network accounts for a large portion of the global river surface area (~ 12%; Raymond et al. 2013), but relatively few studies have been conducted there, with present studies lacking time-series measurements that can document seasonal variation (Marwick et al. 2014; Teodoru et al. 2015; Mwanake et al. 2019). Temperate studies have shown that land use and landcover both affect greenhouse gas emissions (Bodmer et al. 2016; Borges et al. 2018), and the present and on-going rapid land use/land cover change and agricultural intensification in Africa suggests the need for more measurements that cover longer time scales, a wider range of stream sizes, and different landscapes in order to better constrain both regional and global riverine greenhouse gas emission estimates.

Land use and land cover affect greenhouse gas emissions in riverine ecosystems, with agriculture having as much as five times higher emission rates than forested streams, likely due to increased availability of nutrients and labile organic carbon

Additional Supporting Information may be found in the online version of this article.

(Bodmer et al. 2016; Mwanake et al. 2019). Despite this general trend, forested streams may also be significant sources of N_2O (Audet et al. 2019) as well as CH_4 and CO_2, particularly when they drain wetland-dominated catchments (Abril et al. 2014; Borges et al. 2019). These patterns are not well documented in Africa, but may be important due to rapidly increasing deforestation and subsequent agricultural conversion (Winkler et al. 2021). In addition to crop production, livestock watering points in rivers embedded in agro-pastoral and pastoral regions that are common in Africa lead to the alteration of river ecosystems, including deeper pools, longer residence times, and the opportunities for labile organic matter inputs, which likely alter greenhouse gas emissions along the river continuum (Mwanake et al. 2019).

Greenhouse gas emissions from fluvial ecosystems are a function of the delivery of dissolved gasses via sub-surface flow and groundwater inputs and in-stream biogeochemical processes, while the gas transfer velocity controls gas exchange at the air–water interface and therefore regulates when and where the gases are emitted. The gas transfer velocity is partly a function of stream geomorphological variables that affect air–water exchange (turbulence) including slope and stream velocity (Raymond et al. 2012). Within river networks, headwater streams are disproportionately important relative to large rivers (Raymond et al. 2013; Turner et al. 2015) due to their large surface–area-to-volume ratio, which allows close connectivity with the benthic zone and the surrounding landscape (Hotchkiss et al. 2015; Marzadri et al. 2017). Teasing apart these different controls is difficult without process-based studies, but distal factors such as seasonality in hydro-climatic variables (Butman and Raymond 2011), stream size (Hotchkiss et al. 2015; Turner et al. 2015), and land use/land cover (Borges et al. 2018; Mwanake et al. 2019) are important in controlling both the delivery of dissolved gasses to river systems as well as the substrates that are used in the biogeochemical processes responsible for in situ greenhouse gas production (e.g., dissolved inorganic nitrogen [DIN] and dissolved organic carbon [DOC]).

In situ greenhouse gas production is controlled by several biogeochemical processes. Respiration of autochthonous and allochthonous organic carbon produces CO_2 (Battin et al. 2008; Butman and Raymond 2011); methanogenesis in oxygen-depleted stream sediments is responsible for CH_4 production (Duc et al. 2010; Stanley et al. 2016). CH_4 consumption can also occur through aerobic oxidation which may further control methane dynamics in streams (Shelley et al. 2014). N_2O is mainly produced via nitrification and denitrification, although other production processes such as nitrifier-denitrification, dissimilatory nitrate reduction to ammonium, and coupled nitrification–denitrification are also possible sources (Quick et al. 2019). Consumption of N_2O during complete denitrification has also been reported for streams with low nitrate concentrations and high organic carbon availability (Knowles 1982; Baulch et al. 2011b; Mwanake et al. 2019).

Seasonal variation in precipitation and temperature causes variation in riverine greenhouse gas concentration and flux by affecting river discharge (and therefore gas transfer velocities) (Raymond and Cole 2001), water quality parameters, and biogeochemical process rates (Beaulieu et al. 2009; Raymond and Saiers 2010; Marwick et al. 2014). Since temperature fluctuations are relatively small in tropical environments, precipitation is likely the more dominant control compared to temperate systems. Precipitation during wet seasons can lead to supersaturation of greenhouse gases by the direct input of dissolved greenhouse gases to surface waters from the surrounding saturated soils (Yao et al. 2007; Aho and Raymond 2019) and to increasing terrestrial inputs of DOC and dissolved organic nitrogen (DON) (Raymond and Saiers 2010) and DIN (Beaulieu et al. 2009), which may promote in-stream greenhouse gas production. Alternatively, a decrease in greenhouse gas concentrations in surface waters may also occur as a result of dilution with under-saturated terrestrial water inputs (Liu and Raymond 2018) or reduced in-stream production due to lower water residence time and increased gas evasion at high discharge rates (Marwick et al. 2014; Raymond et al. 2016).

Understanding the effects of seasonality, stream order, and catchment land use/land cover on spatial–temporal variation in river-basin greenhouse gas emissions is essential in order to quantify basin-scale emissions. Riverine greenhouse gas studies differ substantially in up-scaling techniques for basin-wide estimates, with most studies using stream orders as a basis for basin-wide estimates (Johnson et al. 2008; Turner et al. 2015; Zhang et al., 2020). Other studies include land use/land cover (Wallin et al. 2018; Audet et al. 2019), while very few take into account the dynamic nature of stream surface areas and fluxes related to varying discharge conditions (see Allen et al. 2018) and spatial heterogeneities along stream reaches (but see Rocher-Ros et al. 2019). Improved up-scaling techniques that incorporate the spatial–temporal heterogeneities in stream surface areas and fluxes are therefore needed to constrain uncertainties of basin wide estimates and improve regional and global greenhouse gas budgets.

The overall objective of this study was to estimate basin-scale greenhouse gas emissions (CO_2, CH_4, and N_2O) from the Mara River Basin in Kenya. The specific objectives were: (1) to evaluate the intra-annual variability of CO_2, CH_4 and N_2O concentrations and fluxes from streams of different sizes draining forests and agricultural ecosystems; (2) to evaluate the effect of seasonality of stream discharge on greenhouse gas concentrations and fluxes, and its influence on in-stream processes vs external inputs sources; and finally (3) to estimate basin-wide riverine emissions taking into account the seasonal variability of discharge and greenhouse gas concentrations.

Materials and methods

Study area

The study was carried out in the Kenyan part of the Mara River catchment (~ 8400 km^2) (Fig. 1; Supporting Information
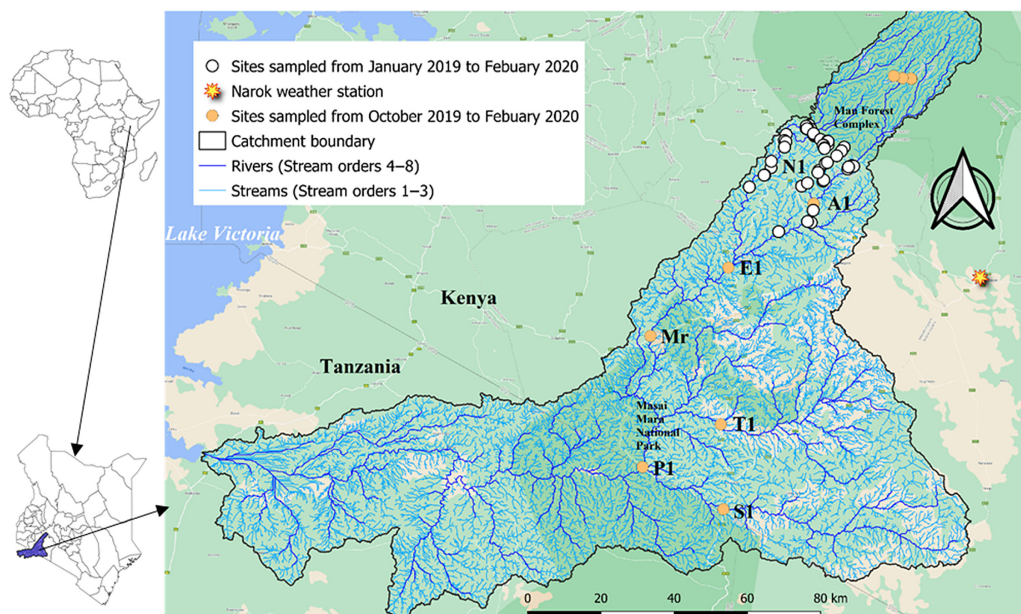
Fig. 1. Map showing the study catchment and its location in Kenya. White and orange dots show sampled points. Points with white dots were sampled monthly from January 2019 to February 2020, and points with orange dots were sampled monthly from October 2019 to February 2020. Labels S1, P1, T1, Mr, E1, N1, and A1 represent sampling points of larger stream orders (6–8). The sampling campaigns were limited to the Kenyan border to Tanzania, but the whole Mara catchment was used to scale up estimates of greenhouse gas emissions. The Mara River remains an 8th order river from the Kenyan border to the mouth at Lake Victoria.

Table S1). The headwaters originate from the protected Mau Forest complex ~ 2900 m above sea level (a.s.l.) and descend through mixed use agriculture and rangeland before crossing the Kenyan–Tanzanian border in the Maasai Mara National Park ~ 1400 m a.s.l. The upper catchment is formed by the two main tributaries—the Nyangores River (N1) and the Amala River (A1), and the middle section starts downstream of the confluence of these two tributaries where it forms the main stem of the Mara River at Emarti (E1) and Mara-Rianta (Mr). Two more tributaries, the Talek (T1) and the Sand River (S1), join the Mara main stem before it crosses the border at Purungut bridge (P1) within the Maasai Mara National Park (Fig. 1; Supporting Information Table S1).

There is a rainfall gradient within the catchment as a result of convectional rainfall, with higher precipitation and lower temperature in the upper catchment (mean annual precipitation ~ 1400 mm and 18°C [range: 9–29°C]) and hotter, drier conditions in the lower catchment (< 1000 mm and 25°C [range 10–31]) (Mati et al. 2008; Dutton et al. 2019). This variation results in a gradient of land cover and agricultural systems, with small remnants of native forest and commercial tea plantations dominating in the upper catchment and agro-pastoral systems with a mix of smallholder food crops (mostly maize) and rangelands for livestock in the middle catchment. The lower part of the catchment is dominated by savannah grasslands, which support the wildlife in the Maasai Mara National Park.

The typical rainfall pattern is bimodal with the first rainy season occurring from March to June ("the long rains") and second rainy season ("the short rains") from October to end of December. The other months are mostly dry with little or no rainfall. The precipitation patterns in the study year (2019) were substantially different from the average year. The first rainy season was delayed and shortened, lasting from May to June, and the second rainy season was heavier (by > 180%) and longer than average, lasting to February 2020. The months of March to April, which normally would have been the start of the first rainy season, were instead the warmest and driest of the year (Fig. 2a).

Overall sampling strategy and sub-catchment characterization

Fifty-nine stream sites covering stream orders 1–8 were selected in a nested catchment design in order to reflect the variation in land use/land cover across the stream orders of the study area (Supporting Information Tables S1, S2). Sampling was conducted monthly from 15 January 2019 to 15 February 2020 using a synoptic survey approach for 47 sites, except for 2 months (February 2019 and January 2020), when no sampling was conducted due to logistical constraints. Twelve additional sites mostly at higher stream orders (7–8) were sampled monthly from October 2019 to February 2020. Individual sub-catchments were delineated using the upslope interactive tool, System for Automated Geoscientific Analyses (SAGA), in QGIS from a Digital Elevation Model with a 30 m resolution (Arc 1) obtained from the Shuttle Radar Topography Mission (retrieved 01 March 2020, link). Sub-catchment
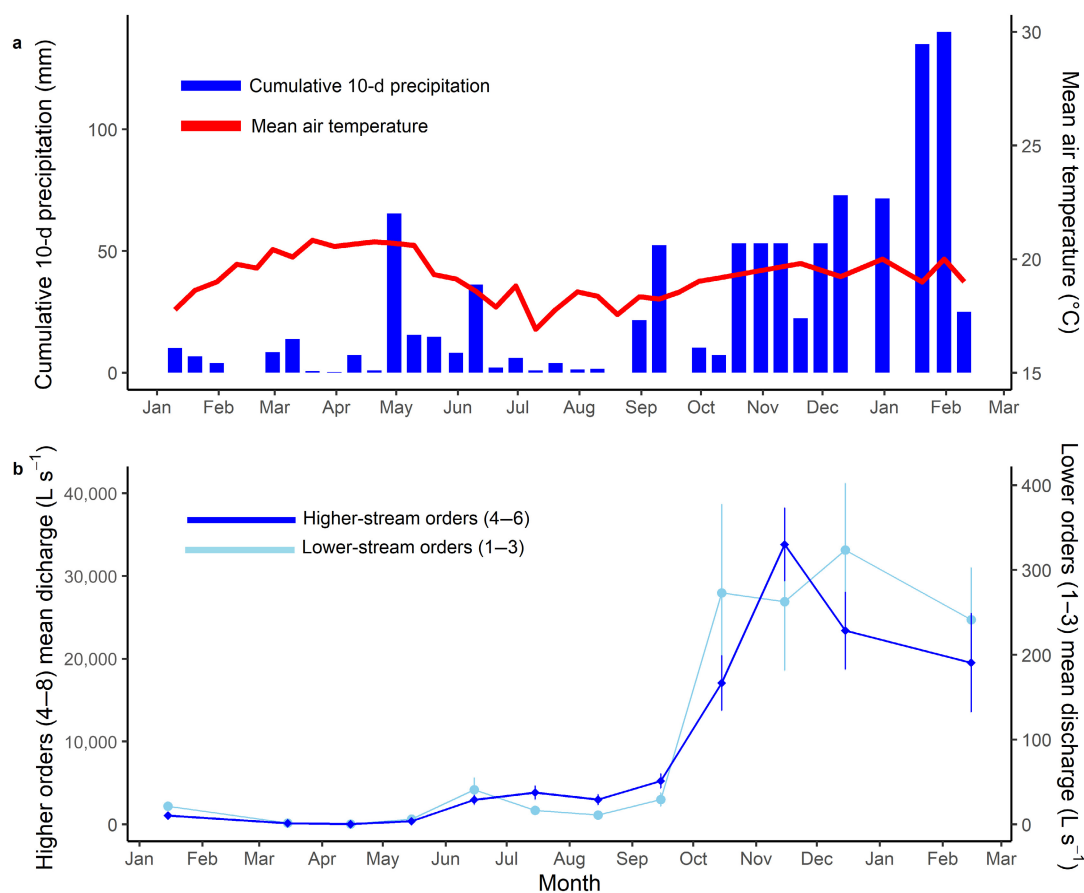
Fig. 2. (**a**) Mean monthly air temperature and precipitation during the study period (January 2019 to February 2020) as recorded by the Kenyan Meteorological Service at the Narok station. (**b**) Mean (±SE) monthly stream discharge for lower-order and higher-order streams in the Mara River.

land-use percentage was calculated from a Sentinel-2 prototype land cover map for Africa with a 20 m by 20 m resolution (retrieved 01 March 2020, link). We focused on the forest and cropland classification within the Sentinel database as the main categories that likely influence greenhouse gas emissions. Urban or artificial areas were not considered as they form <0.1% of the basin area (<5% for any sub-basin). For the purposes of some of the statistical analyses, sites were classified as forest or cropland if these areas comprised > 70% of the basin area or as mixed if the dominant land use/land cover classes comprised < 70%. Stream sites that were used as livestock watering holes by local farmers were classified as livestock sites and were included as an additional "land-use" category (Mwanake et al. 2019).

Stream hydrological and geomorphological characteristics

At each sampling point in small streams, stream velocity was quantified using an electromagnetic sensor (OTT-MF-Pro, Germany); stream width and depth were measured on site, and discharge was calculated by the velocity area method (Gore 2007). For larger rivers that were not wadeable, we also applied the velocity-area method, but acquired

the width using a laser rangefinder (Nikon Model: 8381), measured velocity using floating oranges, and measured depth using permanently installed staff gauges of the Kenyan government (which are not instrumented). At each sampling location, the slope of the stream was measured for each site using a laser rangefinder (Nikon Model: 8381) over a ~5 m reach.

Greenhouse gas sampling and analysis

Gas samples were collected in duplicates using the headspace equilibration technique (Raymond et al. 1997). Triplicate sampling was not feasible due to logistical constraints; however, the coefficient of variation in the duplicates was consistently < 5% for CO_2, < 4% for CH_4, and < 2% for N_2O concentrations. Eighty milliliters of stream water were drawn into a 120-mL syringe with 30 mL of ambient air and equilibrated by shaking under water for 2 min. After equilibration, a 15 mL sample was transferred to a 10 mL pre-evacuated vial for laboratory analysis, which was conducted within few days after sampling at the Mazingira Laboratory (International Livestock Research Institute, Nairobi Kenya). Atmospheric air samples were taken thrice (morning, afternoon, and evening) on

each sampling day to correct for background atmospheric greenhouse gas concentrations in the headspace. The headspace equilibration technique may affect the accuracy of CO_2 measurements for most under-saturated freshwater ecosystems with pH values > 7.5 due to shifts in the carbonate system during equilibration (Koschorreck et al. 2021). This error was assumed minimal and not corrected as the mean pH was 7.3, and CO_2 was consistently oversaturated (mean; 1600 μatm). Greenhouse gas concentrations were analyzed using a gas chromatograph (SRl 8610C) with an electron capture detector for N_2O and a flame ionization detector with a methanizer within the carrier gas stream to allow for simultaneous measurements of CH_4 and CO_2 concentrations.

Greenhouse gas concentrations in the stream water were calculated from the sum of the post-equilibration gas concentrations in the headspace ($C_{post,h}$) and in the water ($C_{post,w}$), after correcting for gas concentrations in atmospheric gas samples ($C_{pre,h}$) (Eq. 1) (Aho and Raymond 2019). Headspace gas concentration was calculated using the Ideal Gas Law. Water-phase gas concentration was calculated using Henry's law (Eq. 2), where C is the gas concentration in water in moles L^{-1}, P is the partial pressure of the gas in atm (mixing ratio in ppmv from GC × atmospheric pressure), and K_h is the Henrys solubility constant for CO_2 (Weiss 1974), N_2O (Weiss and Price 1980), and CH_4 (Wiesenburg and Guinasso 1979).

$$C = C_{post,w} + C_{post,h} - C_{pre,h}, \qquad (1)$$

$$C = PK_h \qquad (2)$$

Daily areal fluxes of all three gasses (CO_2, CH_4, and N_2O,) were calculated using Fick's law of gas diffusion, where the flux is the product of gas transfer velocity (k) in m d^{-1} and the difference between the stream water (C_{aq}) and the atmospheric equilibrium concentration (C_{sat}) in moles m^{-3} for the respective gasses (Eq. 3) and ultimately expressed in units of mass.

$$F = k \left(C_{aq} - C_{sat} \right). \qquad (3)$$

The temperature-specific gas transfer velocities (k) for each of the gases were calculated from normalized k_{600} values in m d^{-1} and temperature-dependent Schmidt numbers (Sc) of the respective gases (Eq. 4), which was suitable according to the range of data presented in the Raymond et al. (2012) dataset and k_{600} results consistent with the energy dissipation model of turbulent streams and rivers.

$$k = k_{600} \left({600}/{Sc} \right)^{0.5}, \qquad (4)$$

$$k_{600} = VS^{0.76} \times 951.5. \qquad (5)$$

Water sampling and analysis

At the time of gas sample collection, water temperature ($^\circ$C), specific conductivity (μS cm^{-1}), dissolved oxygen (DO) (mg L^{-1}), and pH were measured in situ using the Pro DSS multiprobe (YSI Inc.). Water samples for nitrate and ammonium (NO_3-N and NH_4-N) and DOC were collected using 60 mL syringes and filtered on site through pre-combusted (500°C for 4 h) Whatman GFF glass fiber filters (0.7 μm pore size). Samples were collected in acid-washed and pre-leached (with deionized water) high density polyethylene (HDPE) sample bottles for ammonium, nitrate and DOC analysis. DIN samples were refrigerated at 4°C until analysis in the Mazingira Laboratory (within 5 d after collection), and DOC samples were frozen. DIN concentrations were determined using colorimetric methods using an EPOCH microplate spectrophometer (BioTek-Inc.), with NO_3 concentrations analyzed using the Griess reagent (Patton and Kryskalla 2011), and NH_4 using the indophenol method (Bolleter et al. 1961). DOC samples were pre-treated with 10% HCL and concentration measured using the Shimadzu TOC-L analyzer at either Justus Liebig University, Giessen Germany, or ETH, Zurich Switzerland.

Fine benthic organic matter percentage (FBOM%) was determined using the loss on ignition method (Schumacher 2002). Fifteen sediment samples were collected at 0–5 cm depth within a 5 m length of stream using a 3.5 cm diameter sediment corer. The samples were stored in the refrigerator at 4°C for < 5 d before laboratory analysis. Sediments were first sorted to remove large organic debris and macroinvertebrates, and then dried for 24 h at 105°C and finally sieved through a 2-mm sieve. Sub-samples (0.1–0.5 g) of the fine sediments were ashed in a muffle furnace (Nabertherm 30–3000°C) at 550°C to determine percent organic matter.

Seasonality based on discharge

Periods of low, medium, and high discharge were classified based on the normalized discharge values for each site. We normalized discharge measurements as a percent of the maximum discharge at each site, whereby low discharge periods ranged from 0% to 33% of maximum; medium from 34% to 66%; and high from 67% to 100% (Supporting Information Table S2). There were two reasons behind this classification. First, it enabled comparisons of seasonal influences across streams of different sizes and discharge; and second, it was used for up-scaling greenhouse gas emissions to annual fluxes for the whole catchment area.

Statistical analysis

The influence of discharge, stream orders, and land use/land cover on water quality variables, gas concentrations and fluxes were analyzed using a mixed linear regression model-building procedure developed by Zuur et al. (2007). In brief, the procedure first developing a multiple linear regression model by systematically testing combinations of predictor variables that yield the highest R^2 through manual addition and removal of predictor variables, and then using additional random effects (intercept and slope) to assess

model performance based on the value of the Akaike Information Criterion (AIC) values. Predictor variables included cropland %, forest %, and livestock presence (yes or no), stream order and discharge (low, medium, high). Predictor variables that were closely related (with Pearson correlation coefficient > 0.5) were not included in the model. Because cropland and forest % were closely related, we also tested the ratio of cropland to forest as a predictor variable. The results of the traditional multiple linear regression model development ("Model 1") was used as a foundation to develop a mixed model "Model 2," in which we systematically tested the influence of random effects of site and elevation and the possible dependency due to multiple measurements in time (nlme package in R software Version 3.6.1). Of these, we selected the best-fit model based on the AIC value and distribution of residuals. Most of the time, the best-fit "Model 2" included a random effect of site, and this was also the better model compared to Model 1 based on AIC and residual distributions. A Tukey post hoc analysis (p-value < 0.05) was then used to identify individual differences within each grouping factor for categorical fixed effects. When necessary, dependent data were transformed using the natural logarithm to meet the assumption of normality, and this included greenhouse gas concentrations, flux, and some water quality data.

To infer to possible biogeochemical processes responsible for CO_2, CH_4, and N_2O concentrations, their relationships with different water quality parameters were assessed using a multiple linear regression model with manual stepwise removal of the insignificant independent variables. The initial parameters of the model included DO, DOC, FBOM%, and NH_4-N and NO_3-N. These parameters were chosen for the analysis because they represent direct drivers of biogeochemical processes. Collinearity for the independent variables was checked before running the models, with a < 50% correlation threshold defined for choosing the final predictor variables to be included in the models.

Basin-wide estimate of greenhouse gas fluxes

We estimated greenhouse gas emissions for the whole Mara River (including the Tanzanian side), by multiplying the measured greenhouse gas fluxes by wetted area. The Zonal statistics tool in QGIS was used to sum the total stream length for each stream order (Strahler (1952) classification) in the basin, yielding a total of 17,636 km for the basin (orders 1–8). As flux data were lacking for 4th and 8th order streams, the lengths for these orders were added to 5th and 7th orders, respectively. The stream surface area by stream order was calculated as a product of the stream lengths and the mean widths measured in the field campaigns at low, medium, and high discharge periods.

Areal fluxes of the greenhouse gases were calculated for the three different discharge periods by multiplying the mean stream surface area with the mean greenhouse gas flux measured during that period and the number of days within that period. The number of days in each discharge period was based on the monthly discharge data, and this resulted in 60 d of low discharge (March and April), 185 d of median discharge (January, May, June, July, August, and September) and 120 d of high discharge (October, November, December, and February 2020) (Fig. 2). Whole basin fluxes were calculated by summing the emissions of the low, medium, and high discharge periods for each stream order. A sensitivity analysis was carried out to determine whether the largest uncertainties in whole-basin estimates were due to surface area (i.e., the width associated with low, medium, and high discharge), fluxes, or a combination of both. The total-basin emissions are presented for CO_2, CH_4, and N_2O and as CO_2 equivalents based on GWP, that is, 28 and 298 for CH_4 and N_2O, respectively (IPCC 2014).

Results

Seasonal variability of hydrology and water quality variables

Stream/river discharge across all sites ranged from 0.02 to 71,500 L s^{-1} during the study period. The mean monthly values ($\pm$ SE) across all stream orders spanned over four orders of magnitude, with the lowest mean discharge (8.06 $\pm$ 3.61 L s^{-1}) observed in April during the period of delayed rains and the largest discharge values (10,100 $\pm$ 2560 L s^{-1}) observed in November during the second rainy season (Fig. 2b). The ranges for water quality variables were: water temperature 11–34°C; DO 0.7–10.8 mg O_2 L^{-1}; NO_3-N 0.18–18.21 mg N L^{-1}; DOC 0.80–25.03 mg C L^{-1}; and FBOM 0.11–23.09%. The lowest mean monthly values across stream orders for DO and NO_3-N concentrations were in the low-discharge months of March and April, and were 1.25 times lower for DO and four times lower for NO_3-N than the high-discharge months (October to February) (Fig. 3). DOC and FBOM showed the opposite pattern, with the highest concentrations in March and April and the lowest in October to February (Fig. 3). DO and NO_3-N concentrations were generally slightly higher in the medium and high discharge periods, while DOC concentrations were twofolds lower in the same period compared to the low discharge period (Tables 1, 2; Supporting Information Fig. S1).

Seasonal variability of greenhouse gas concentration and flux

Throughout the study period, CO_2 and N_2O concentrations spanned over two orders of magnitude ranging from 82 to 4000 μg-C L^{-1} (pCO$_2$; 192–8009 μatm) and from 95 to 3890 ng N L^{-1} (pN$_2$O; 120–4920 natm), respectively, while CH_4 had the most variation spanning over five orders of magnitude, that is, 0.04–449 μg C L^{-1} (pCH$_4$; 3–30,700 μatm). CH_4 concentrations decreased with discharge (Tables 1, 2; Supporting Information Fig. S2), with the highest mean monthly values in March and April and the lowest in October to February
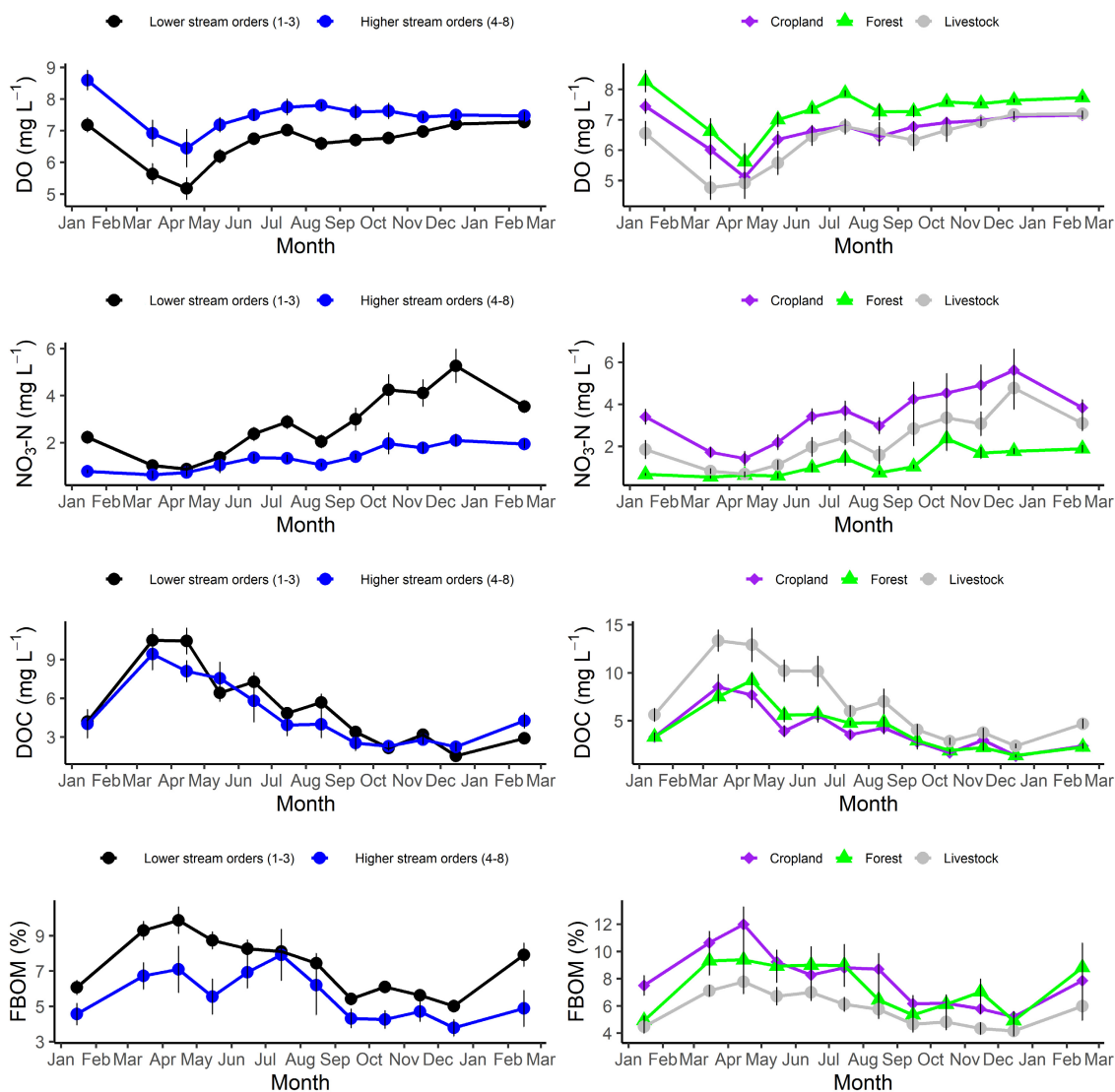
Fig. 3. Monthly trends of DO, NO_3-N, DOC concentrations, and FBOM (%) grouped by stream order (1–3, 4–8) and land use/land cover class (see methods for classification criteria). Points and error bars represent mean monthly values $\pm$ SE (Supporting Information Table S2).

(Fig. 4). This seasonal trend was opposite for N_2O concentrations, which slightly increased at high discharge (Tables 1, 2; Supporting Information Fig. S1), while CO_2 concentrations were not related to discharge (Tables 1, 2; Supporting Information Fig. S1).

Overall, streams were mostly net sources of all three greenhouse gases to the atmosphere, but there were a few occasional sinks of CO_2 and N_2O, especially in higher stream orders during low discharge conditions. CO_2 and N_2O fluxes ranged from -1720 to $61,900$ mg C m^{-2} d^{-1} (mean = 3740 mg C m^{-2} d^{-1}) and from -1510 to $32,800$ μg N m^{-2} d^{-1} (mean = 1570 μg N m^{-2} d^{-1}), respectively. CH_4 fluxes spanned over five orders of magnitude, ranging from 0.06 to 492 mg C m^{-2} d^{-1} (mean = 33 mg C m^{-2} d^{-1}). Generally, all three greenhouse gas fluxes increased with increasing stream

discharge, similar to the gas transfer velocity (Tables 1, 2; Fig. 5). The highest fluxes were at highest discharge conditions in the second rainy season from October to February, while the lowest fluxes were mostly in the other months. Mean monthly CO_2 and N_2O fluxes spanned up to two orders of magnitude between the lowest and the highest months, while CH_4 fluxes showed a much smaller monthly variation (Fig. 5).

Effect of stream order and land use/land cover on water quality parameters

Stream order had no effect on DOC, but had a positive relationship with DO and a negative relationship with NO_3-N concentrations and FBOM % (Table 1). NO_3-N concentrations were on average two times higher for stream orders 1–3 than for stream orders 4–8, while DO concentrations only slightly

Table 1. Results of multiple linear mixed effects models (Model 2; *see* "Statistical Analysis" section) predicting the effect of stream order, land use/land cover (%), discharge (low, medium, high) and livestock (presence/absence) on water and sediment variables, k_{600}, CO_2, CH_4, and N_2O concentrations and fluxes. The + and − signs beside the slope estimates indicate the direction of the relationships. CRP denotes % cropland, and CRP : FOR denotes cropland to forest ratio. Asterisks denote the significance level with * $p<0.05$; ** $p<0.01$; *** $p<0.001$; n.s. > 0.05.

Type 2 ANOVA table

Includes Wald chi-sq. statistic, p-values, and slope parameter estimates of predictor variables and their interactions

| Dependent variables	Stream order Chi-sq. statistic	Stream order Slope ± SE	CRP or CRP : FOR Chi-sq. statistic	CRP or CRP : FOR Slope ± SE	Discharge (Q) Chi-sq. statistic	Discharge (Q) Slope ± SE	Livestock Chi-sq. statistic	Livestock Slope ± SE	Interactions CRP or CRP : FOR * Q	Interactions Livestock * Q
Water quality and sediment variables										
DO (mg L^{-1})	5.3*	0.11 ± 0.05	7.6**	−0.006 ± 0.002	150,910***	0.0003 ± 0.0001	4.4*	−0.37 ± 0.19	n.s.	12.9**
NO$_3$-N (mg L^{-1})†	13.8***	−0.13 ± 0.04	22.8***	0.009 ± 0.002	22.9***	0.005 ± 0.0007	n.s.		n.s.	7.8*
DOC (mg L^{-1})†	n.s.	−0.11 ± 0.03	n.s.		72.6***	−0.008 ± 0.0007	20.7***	0.45 ± 0.10	n.s.	6.9*
FBOM %†	100.8***		n.s.		25.7***	−0.003 ± 0.0004	7.2**	−0.12 ± 0.05	n.s.	n.s.
Gas concentration and flux										
CO$_2$ concentration (µg C L^{-1})†	43.1***	−0.21 ± 0.03	n.s.		n.s.		n.s.		11**	n.s.
CH$_4$ concentration (µg C L^{-1})†‡	25.6***	−0.33 ± 0.06	n.s.		15.5***	−0.002 ± 0.001	34.8***	1.19 ± 0.24	42.7***	n.s.
N$_2$O concentration (mg N L^{-1})†	22.6***	−0.12 ± 0.02	13.3***	0.005 ± 0.001	30.1***	0.002 ± 0.0002	n.s.		8.6*	7.3*
k$_{600}$ (m d^{-1})	n.s.		n.s.		511.1***	0.11 ± 0.0003	n.s.		10.2**	5.9
CO$_2$ flux (mg C m^{-2} d^{-1})†	45.5***	−0.16 ± 0.02	12.1***	0.003 ± 0.001	171.6***	0.009 ± 0.0006	14.7***	0.33 ± 0.08	7.2*	8.5*
CH$_4$ flux (mg C m2 d^{-1})†‡	7.3**	−0.20 ± 0.07	n.s.		32.9***	0.01 ± 0.001	22.1***	1.20 ± 0.27	35.7***	n.s.
N$_2$O flux (µg N m^{-2} d^{-1})†‡	17.7***	−0.11 ± 0.03	15.1***	0.004 ± 0.001	107.6***	0.006 ± 0.0005	n.s.		n.s.	8.1*

†Natural logarithm transformation (1515 and 1725 were added to N$_2$O and CO$_2$ fluxes, respectively, to remove the negatives).
‡Used CRP : FOR.

Table 2. The effect of discharge and livestock presence on water and sediment parameters, k_{600}, and greenhouse gas concentrations and fluxes. The bold letters (**a** and **b**) beside the means ($\pm$SE) represent significant differences in grouping factors based on Tukey post hoc analysis results from the linear mixed effects model (Model 2; Table 1).

	Discharge periods mean $\pm$ SE			Livestock presence mean $\pm$ SE	
	Low	**Medium**	**High**	**No**	**Yes**
Water and sediment variables					
DO (mg L^{-1})	6.8 $\pm$ 0.1 **a**	7.3 $\pm$ 0.1 **b**	7.3 $\pm$ 0.1 **b**	7.1 $\pm$ 0.1 **b**	6.5 $\pm$ 0.1 **a**
NO$_3$-N (mg L^{-1})	2.1 $\pm$ 0.1 **a**	3.5 $\pm$ 0.3 **b**	3.8 $\pm$ 0.4 **b**	2.5 $\pm$ 0.1 **a**	2.9 $\pm$ 0.2 **a**
DOC (mg L^{-1})	5.4 $\pm$ 0.2 **b**	2.2 $\pm$ 0.2 **a**	2.5 $\pm$ 0.2 **a**	3.9 $\pm$ 0.2 **a**	6.2 $\pm$ 0.3 **b**
FBOM	7.0 $\pm$ 0.2 **b**	6.5 $\pm$ 0.6 **ab**	5.7 $\pm$ 0.3 **a**	7.3 $\pm$ 0.2 **a**	5.6 $\pm$ 0.2 **a**
Gas concentration and flux					
CO$_2$ concentration (μg C L^{-1})	810.9 $\pm$ 27.6 **a**	695.1 $\pm$ 69.9 **a**	753.7 $\pm$ 53.4 **a**	863.4 $\pm$ 30.6 **a**	686.3 $\pm$ 30.9 **a**
CH4 concentration (μg C L-1)	8.9 $\pm$ 0.9 **b**	3.8 $\pm$ 1.5 **a**	2.5 $\pm$ 0.2 **a**	6.6 $\pm$ 0.8 **a**	13.3 $\pm$ 2.6 **b**
N$_2$O concentration (ng N L^{-1})	429.2 $\pm$ 18.2 **a**	499.7 $\pm$ 74.9 **a**	506.6 $\pm$ 45.7 **b**	490.8 $\pm$ 23.8 **a**	375.8 $\pm$ 15.1 **a**
k_{600} (m d^{-1})	5.9 $\pm$ 0.3 **a**	11.5 $\pm$ 1.0 **b**	16.6 $\pm$ 1.1 **c**	8.9 $\pm$ 0.5 **a**	8.7 $\pm$ 0.5 **a**
CO$_2$ flux (mg C m^{-2} d^{-1})	2573 $\pm$ 196 **a**	3546 $\pm$ 656 **b**	7318 $\pm$ 999 **c**	4364 $\pm$ 384 **a**	2580 $\pm$ 242 **a**
CH$_4$ flux (mg C m^{-2} d^{-1})	32.3 $\pm$ 2.8 **a**	20.2 $\pm$ 2.4 **a**	36.8 $\pm$ 4.6 **b**	27.2 $\pm$ 2.3 **a**	44.1 $\pm$ 4.7 **b**
N$_2$Oflux (μg N m^{-2} d^{-1})	997.9 $\pm$ 153.2 **a**	1989.8 $\pm$ 573.2 **b**	3316.2 $\pm$ 584.6 **c**	1919.9 $\pm$ 243.6 **a**	933.7 $\pm$ 145.9 **a**
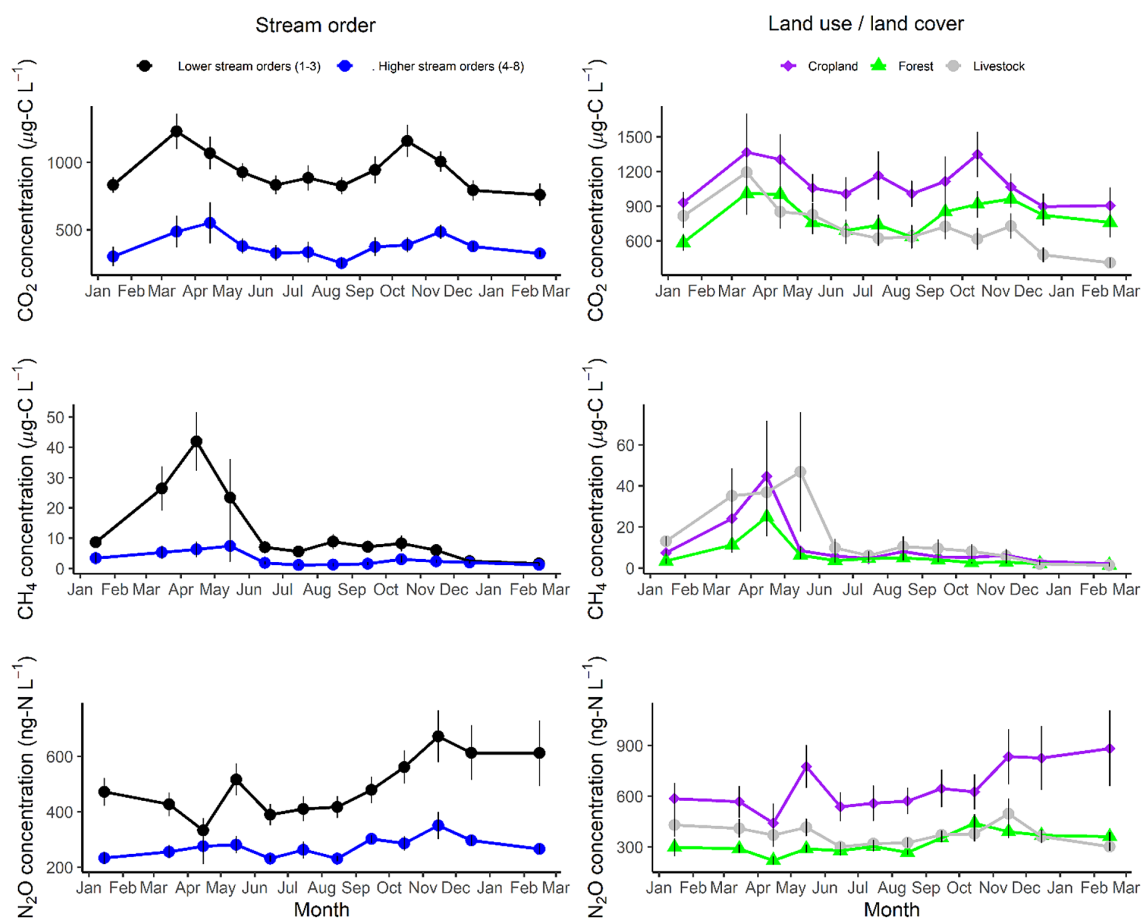
Fig. 4. Monthly trends of CO$_2$, CH$_4$, and N$_2$O concentrations grouped by stream order (1–3, 4–8) and land use/land cover class (*see* "Materials and Methods" section for classification criteria). Points and error bars represent mean monthly values $\pm$ SE (Supporting Information Table S2).
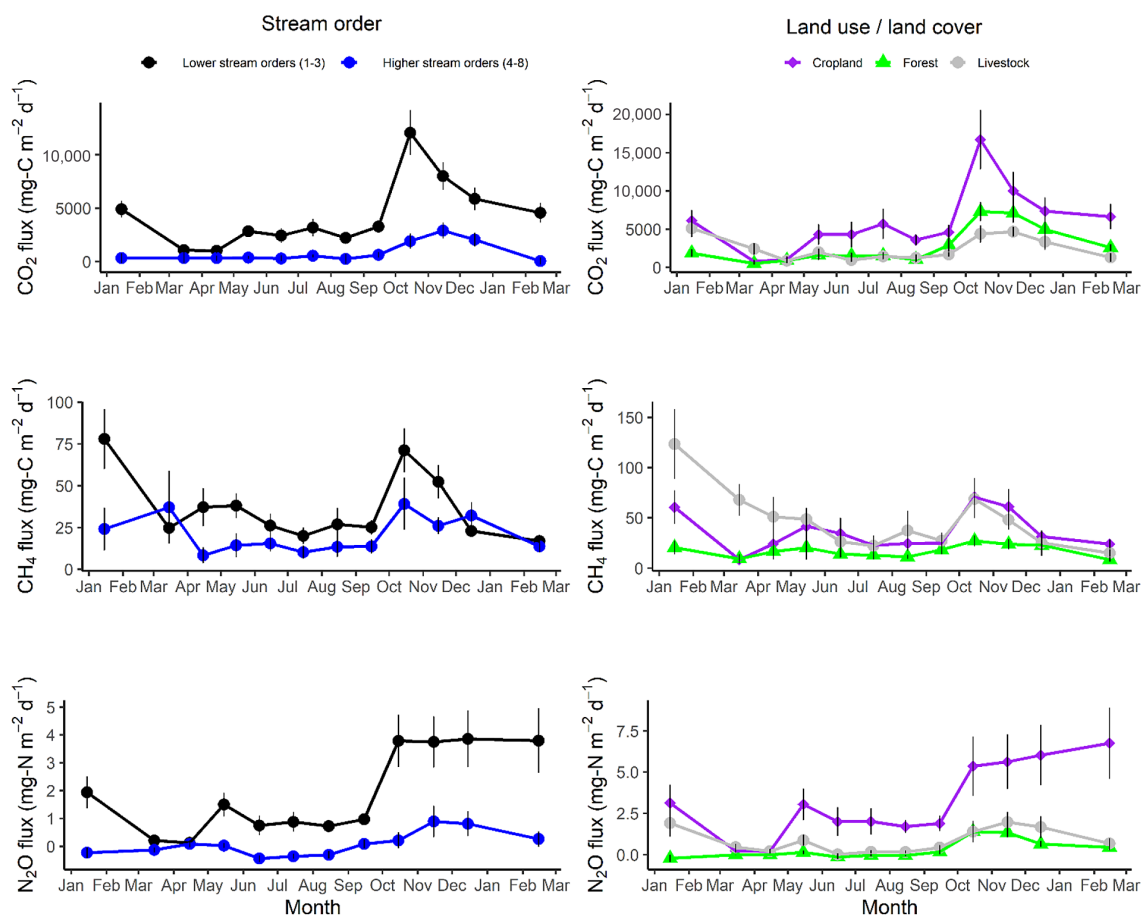
Fig. 5. Monthly trends of CO_2, CH_4, and N_2O fluxes grouped by stream order (1–3 and 4–8) and land use/land cover class. Points and error bars represent mean monthly values $\pm$ SE (Supporting Information Table S2).

increased from low- to high-stream orders (Fig. 3). Cropland percentage in the sub-basin drainage area had a positive relationship with NO_3-N and a negative one with DO concentrations (Table 1; Fig. 3). Stream sites with livestock presence had higher DOC, DO, and lower FBOM% than those without (Tables 1, 2; Fig. 3). There was also a significant interaction between discharge and livestock presence on water quality parameters, where the presence of livestock had a stronger negative effect on DO, and a stronger positive effect on DOC during the low discharge period (interactions in Table 1; Supporting Information Fig. S3).

Effect of stream order and land use/land cover on greenhouse gas concentration and fluxes

CO_2, CH_4, and N_2O concentrations showed a decreasing trend with stream order (Table 1; Fig. 4). CO_2 and N_2O concentrations were on average ~ twofold higher in the lower-order streams than in higher orders, while CH_4 concentrations were five times higher in the lower-order streams than higher orders (Fig. 4). Fluxes mostly followed a similar trend as concentrations and decreased with increasing stream orders

(Table 1; Fig. 5). Land use/land cover also significantly influenced gas concentrations and fluxes, with increasing N_2O concentrations and fluxes increasing cropland %. CH_4 concentrations and fluxes were ~ 2 times higher at stream sites with livestock presence (Tables 1, 2; Figs. 4, 5). CO_2 concentrations also increased with cropland %, but this positive effect was significant only during the low and medium discharge periods (significant interaction; Table 1; Supporting Information Fig. S3). CO_2 fluxes behaved slightly differently, in that fluxes increased with cropland %, irrespective of discharge conditions (Table 1; Supporting Information Fig. S3). Presence of livestock had a negative effect on N_2O concentrations and fluxes, but only during the low and medium discharge periods (significant interaction; Table 1; Supporting Information Fig. S3).

Relationships between water quality parameters and greenhouse gas concentrations

Stream CO_2 concentrations were positively related to FBOM % and DOC concentrations and negatively related to DO (Table 3). CH_4 concentrations were also positively related to

Table 3. Results of simple multiple linear regression models predicting CO_2, CH_4 and N_2O concentrations from DO, NO_3-N concentration, DOC concentration, and FBOM%. *B shows model coefficients (intercept and slope). Asterisks denote the significance level with * p < 0.05; ** p < 0.01; *** p < 0.001; n.s. > 0.05.*

Predictor variables	Log$_e$ normalized gas concentrations								
	CO_2-C concentration (μg L^{-1})			CH_4-C concentration (μg L^{-1})			N_2O-N concentration (ng L^{-1})		
	B	Std. err	*p*-value	*B*	Std.err	*p*-value	*B*	Std. err	*p*-value
(Intercept)	7.84	0.16	***	2.48	0.11	***	6.68	0.11	***
DO (mg L^{-1})	−0.24	0.02	***	−0.6	0.04	***	−0.13	0.02	***
NO_3-N (mg L^{-1})	0.02	0.009	*	−0.11	0.02	***	0.29†	0.02	***
DOC (mg L^{-1})‡	0.02‡	0.007	*	0.15‡	0.01	***	−0.02‡	0.006	**
FBOM %	0.04	0.01	***			n.s.			n.s.
Adjusted r^2		**0.25**			**0.40**			**0.29**	
Model *p*-value		**<2.2e-16**			**<2.2e-16**			**<2.2e-16**	
Degrees of freedom		**518**			**557**			**550**	

†Natural logarithm transformation.
‡Bivariate correlation coefficients due to strong covariation between DO and DOC.

DOC concentrations and negatively related to DO and NO_3-N concentrations (Table 3). N_2O concentrations were positively related to NO_3-N concentrations and negatively related to DO and pH (Table 3). Overall, CO_2 and CH_4 concentrations had stronger relationships with DO, which was responsible for a 24% reduction in CO_2 concentrations and a 60% reduction in CH_4 concentrations relative to the other main predictor variables. NO_3-N was the strongest predictor of N_2O, resulting in a 29% increase in N_2O concentrations for every unit increase. In addition, the strength of the relationships between DO and CO_2 and CH_4 were both highest during the low discharge period, which was also true for relationships between NO_3-N and N_2O and for DOC and CH_4 (Supporting Information Fig. S2).

Up-scaling

Total annual net greenhouse gas emission of the Mara basin was 294 ± 35 Gg CO_2 eq yr^{-1}. CO_2 was the main contributor, accounting for 88% of the total catchment fluxes (259 Gg CO_2 eq yr^{-1}), while N_2O and CH_4 contributed 5% and 7%, respectively (15 and 21 Gg CO_2 eq yr^{-1}, respectively) (Supporting Information Table S5; Fig. 6). Generally, annual fluxes for CO_2, CH_4, and N_2O were an order of magnitude higher in the high and medium discharge periods than the low discharge period, particularly for lower stream orders (1–3) (Supporting Information Table S5). The contribution to the total areal flux generally decreased with decreasing stream order, with lower-order streams (1–3) contributing 81% and higher stream orders (4–8) contributing only 18%. For individual gases, CO_2 and N_2O fluxes from lower-order streams each contributed 83% to their total fluxes, while higher-order streams contributed 17%. These contributions were different for CH_4 fluxes, which showed almost equal contribution from

lower- and higher-order streams (53% and 47%, respectively; Supporting Information Table S5; Fig. 6).

Sensitivity of up-scaled emissions to discharge

We found that ignoring seasonality in discharge in the up-scaling procedure led to an underestimation of the annual fluxes by 36% (Supporting Information Tables S6, S7). Further sensitivity analyses showed high sensitivity of annual flux estimates to width, because width varied seasonally depending on discharge, which in turn had a strong effect on stream surface area (Supporting Information
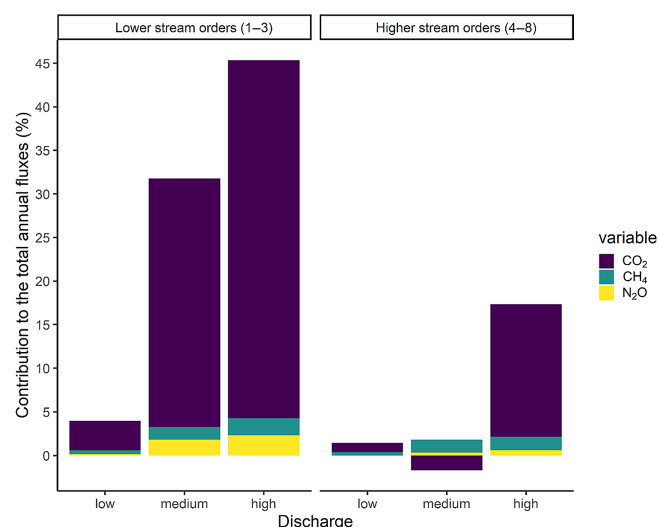
Fig. 6. Contributions of CO_2, CH_4, and N_2O expressed as a percentage to the total emissions in CO_2 equivalents (294 Gg CO_2 eq yr^{-1}) based on low (1–3) and higher (4–8) stream order classes and on low, medium, and high discharge periods.

Table S5). Ignoring the variation in stream surface area alone led to an underestimation of the annual fluxes by up to 28% (Supporting Information Table S7). The effect was strongest in lower-order streams, with fluxes from 1st, 2nd, and 3rd order streams underestimated by 26% while effects were minor for stream orders > 4 (Supporting Information Table S7). Using mean annual fluxes rather than seasonally weighted fluxes from discharge periods introduced lower uncertainty, with total catchment fluxes affected by less than 14% (Supporting Information Table S7).

Discussion

Overall trends

In agreement with findings from other studies on African rivers, the Mara river basin is a net source of greenhouse gas emissions to the atmosphere (Table 4), contributing ~ 294 Gg CO_2 eq yr^{-1}. Generally, the spatial and temporal variation of CO_2, CH_4, and N_2O concentrations and fluxes in this study were linked to seasonality in stream discharge, stream order, and land use/land cover. Temporal changes in greenhouse gas concentrations and fluxes were related to the balance between instream processing, which dominated during the low discharge season, and increased external supply and high evasion rates, which dominated during the medium and high discharge seasons. During the low discharge period, the different gases acted differently with respect to super-saturation or under-saturation (discussed below for the individual gases). During the high discharge period, CO_2 and N_2O fluxes were up to three times higher, indicating that increased supply from external sources could offset the reduction in instream production rates. Catchment characteristics such as the dominant land use/land cover and stream size influenced the spatial variability in greenhouse gas concentrations and fluxes. Cropland and livestock streams, which were characterized by higher temperatures and higher nutrient and organic matter concentrations than forested streams, favored instream production of the greenhouse gases resulting in higher fluxes, while lower-order streams with better sediment–water and land–water connectivity also exhibited higher fluxes.

CO_2 concentration and flux

The seasonal trends of CO_2 concentrations and fluxes in our study were linked to changes in discharge and to seasonal patterns of organic carbon (DOC and FBOM%), observations which agree well with other studies (Bodmer et al. 2016; Borges et al. 2018; Wallin et al. 2020). Our data show that increased organic carbon concentration and low gas evasion rates during low discharge periods may have favored an increase in microbial heterotrophic production of CO_2, sustaining oversaturated concentrations. This finding is supported by the positive relationship of CO_2 concentration with DOC concentration and FBOM%, and the strong

negative relationship with DO. Borges et al. (2018) in their study of seasonal dynamics in greenhouse gas concentration in the Meuse catchment, Belgium, also attributed high CO_2 concentrations in the low discharge summer months to in situ microbial production processes and the reduction of the gas transfer velocity under low discharge conditions.

CO_2 concentrations in the high discharge period were supersaturated and were not in equilibrium as might be expected for turbulent rivers with high gas evasion rates (k). This finding may indicate external inputs of dissolved CO_2 from terrestrial sources. Liu and Raymond (2018) in their study of streams and rivers in the conterminous United States found that half of the sites showed a positive correlation between CO_2 concentrations and discharge, which was attributed to terrestrial inputs during periods of precipitation. In our study, the supersaturation combined with the high evasion rates in the medium and high discharge seasons yielded higher fluxes. Similar hydrological controls on increased CO_2 outgassing in high discharge periods have been extensively reported in tropical rivers (Rasera et al. 2013; Almeida et al. 2017; Duvert et al. 2020).

In order to assess the hypothesis that instream production of CO_2 by respiration dominated during the low discharge period while external inputs of dissolved CO_2 from terrestrial sources dominated during the high discharge period, we compared previous measurements of net ecosystem production (NEP) from 10 forested and 10 agricultural lower-order sites (1–3) in the Mara Basin (Masese et al. 2017) with the CO_2 fluxes measured in this study. In a previous study, the mean NEP was ~ 2052 mg CO_2-C m^{-2} d^{-1} in the dry season and ~ 1476 mg CO_2-C m^{-2} d^{-1} in the wet season (Masese et al. 2017). The dry-season measurements of NEP are similar to our measured CO_2 fluxes in the low-discharge period (~2676 mg CO_2-C m^{-2} d^{-1}), suggesting that NEP could have accounted for nearly all (~80%) of the CO_2 flux. In contrast, the wet-season NEP values accounted for a much smaller proportion (~20%) of the CO_2 fluxes that we measured in the high discharge period (~8004 mg CO_2-C m^{-2} d^{-1}). We therefore conclude that it is likely that external sources of CO_2 contributed more to annual stream CO_2 fluxes than instream production. A similar conclusion from 12 other sub-Saharan rivers was reached by Borges et al. (2015).

Land use/land cover also influenced CO_2 concentrations and fluxes, but this effect was strongly affected by discharge. Higher cropland % led to higher CO_2 concentrations, but only at low and medium discharge conditions (Supporting Information Fig. S3), consistent with the idea that NEP at low discharge contributes to a higher portion of CO_2 production than terrestrial inputs. NEP in cropland systems may be higher than in forested systems due to higher temperature and higher nutrient concentrations (Lambert et al. 2017; Drake et al. 2019), which were also shown for our sites (Supporting Information Table S3), as

Table 4. Literature summary of CO_2, CH_4 and N_2O emission estimates from rivers and streams in Africa. The basin-wide riverine emissions are for CO_2 fluxes only as upscaled N_2O and CH_4 data for each river basin was not provided in the Borges et al. (2015) study.

Study site	Main drainage land use (> 50% of catchment area)	Catchment size (km²)	Stream surface area (km²)	Stream surface area: catchment area (%)	Stream orders sampled	Type of study	Duration of study	CO_2 flux (mg-C m⁻² d⁻¹)		CH_4 flux (mg-C m⁻² d⁻¹)		N_2O flux (µg N m⁻² d⁻¹)		Mean catchment CO_2 emissions (Tg C yr⁻¹)	Mean CO_2 emissions in mg C km⁻² of catchment area yr⁻¹	Reference
								Range	Mean	Range	Mean	Range	Mean			
African studies																
This study	Cropland	13,500	65	0.48	1–8	Monitoring	1 yr	−1716 to 61,920	3732	0.06–490	33	−1512 to 32,788	1568	0.08	5.92	This study
Congo	Forest	3,705,222	26,517	0.72	—*	Survey and monitoring	2–60† d, 1–2 yr‡		18,240		222		532	176.5	47.64	Borges et al. (2015)
Zambezi	Woodland and shrubland	1,378,102	7325	0.53	—*	Survey and monitoring	2–60† d, 1–2 yr‡		5052		163.2		56	13.52	9.81	Borges et al. (2015)
Betsiboka	Grassland	68,311	1105	1.62	—*	Survey	2–60† d, 1–2 yr‡		6276		42		252	2.53	37.04	Borges et al. (2015)
Tana River, Kenya	Grassland	100,608	895	0.89	—*	Survey and monitoring	2–60† d, 1–2 yr‡		2376		7.2		168	1.09	10.83	Borges et al. (2015)
Athi-Galana-Sabaki River, Kenya	Grassland	40,300	359	0.89	—*	Survey and monitoring	2–60† d, 1–2 yr‡		3672		16.8		532	0.05	1.24	Borges et al. (2015)

*Mostly large rivers (>100 m width) but order not specified.
†Survey duration.
‡Monitoring duration.

well as by Masese et al. (2017) for cropland systems in the upper Mara. In contrast with CO_2 concentrations, CO_2 fluxes generally increased with cropland % in all discharge periods. Gas exchange rates (k_{600}) increased with cropland % during the high discharge period (Supporting Information Fig. S3i), suggesting that these systems are more flashy and therefore more turbulent compared to forested streams as a result of more sparse upland vegetation cover.

CH_4 concentration and flux

In this study, CH_4 concentrations were highest in the low discharge period, in lower-stream orders, and in livestock sites. We attribute this finding to higher rates of sediment methanogenesis, as evidenced by lower DO, low NO_3-N and high DOC that we observed at the same time (Table 1; Fig. 4), and the strong negative relationship between CH_4 and DO and NO_3 concentration and the positive relationship with DOC (Table 3). During the longer residence times created in low-discharge periods, low gas transfer rates together with the consumption of oxygen and nitrate as terminal electron acceptors and the increased mineralization of organic carbon appears to have provided suitable conditions for methanogenesis. Similar conditions were also related to increased methanogenesis in stream sediments in a global review of riverine methane dynamics (Stanley et al. 2016). These conditions were evident in the livestock sites, which are characterized by deeper pools with slower moving water as well as additional input of organic matter from manure, and in the lower catchment, possibly inputs from other wildlife such as hippos, more common in the Masai Mara Park. Comparable seasonal trends of high CH_4 concentrations in the low discharge periods have also been reported in other tropical rivers in Africa (Koné et al. 2010) and in South America (Sawakuchi et al. 2014), as well as in temperate rivers (Baulch et al. 2011a; Schade et al. 2016).

In contrast, CH_4 concentrations in the medium and high discharge seasons were threefold lower than in the low discharge season. This finding may suggest a possible limitation of sediment methanogenesis, or methanotrophy in more oxygenated sediments or higher methane evasion rates, features which were also observed in previous studies (de Angelis and Scranton 1993; Sawakuchi et al. 2014; Lupon et al. 2019). Fluxes showed the reverse pattern as concentrations, with the highest CH_4 fluxes in the high discharge period, particularly at the lower-order streams (Table 2; Fig. 6), which is possible from external sources of CH_4 due to hydrologically connected water-saturated soils, including seasonally-flooded riparian zones, and also higher gas evasion rates.

N_2O concentration and flux

In contrast with CO_2 and CH_4, N_2O concentrations slightly increased with discharge. Two possible explanations could account for this observation: First, low concentrations of NO_3-N and DO and higher availability of DOC during the low

discharge period may have stimulated complete denitrification to N_2, an interpretation in line with findings of previous studies (Richey et al. 1988; Mwanake et al. 2019). Second, increased inputs of terrestrial NO_3-N (and organic C) in the high discharge period provided substrate for N_2O production by denitrification. This interpretation is further supported by the positive relationship between N_2O and NO_3 concentrations, which were highest during the high discharge season. Beaulieu et al. (2009) in their study of 12 headwater streams in the Kalamazoo basin United States also found peak N_2O and NO_3-N concentrations during rain and snowmelt events, which they also attributed to elevated N_2O production due to terrestrial NO_3-N inflows. N_2O fluxes were an order of magnitude higher in the medium and high discharge periods than in the low discharge period. This finding may suggest similar controls and importance of external sources as identified for CO_2 and CH_4 fluxes, and a combination of supersaturation and higher gas transfer velocities yielding in overall higher fluxes.

Contrary to a previous study in the upper Mara (Mwanake et al. 2019), the decreasing trend of N_2O concentrations and fluxes with stream order in this study was probably due to the difference between discharge conditions during the two studied periods. The study by Mwanake et al. (2019) had discharge ranging from 0.03 to 6990 L s^{-1} for stream orders 1–6, which was on the lower range of values of 0.02–47,663 L s^{-1} reported for this study. The heavy rainfall events that occurred from October 2019 to February 2020 in this study contributed to larger discharge variation and higher gas transfer velocities and increased supply of terrestrial NO_3 particularly to low-order streams, thus accounting for larger differences in N_2O concentrations and fluxes between stream orders. This was also evident from the mean N_2O flux quantified here, which was ∼ 3 times greater than that reported by Mwanake et al. (2019).

Cropland streams with high NO_3-N seemed to support N_2O production processes and subsequent N_2O supersaturation, similar to previous riverine studies that linked high NO_3-N concentrations in cropland streams to N_2O supersaturation (Baulch et al. 2011b; Marwick et al. 2014; Mwanake et al. 2019). On the other hand, low N forested sites (< 3 mg L^{-1} NO_3-N) were characterized by lower N_2O concentrations. Tea farming in the upper Mara region may explain the higher NO_3-N observed in the cropland streams than forested streams. Commercial tea farms in the region apply up to 250 kg ha^{-1} fertilizers nitrogen during the cropping season, which starts before the long (March to June) and short (October to December) rains (Wanyama et al. 2018). This management activity likely supports the overall positive correlation we found between NO_3-N and N_2O concentrations. However, the relationship with NO_3-N was relatively weak and explained only 19% of the variance. One possible explanation for the weak correlation could be that external sources of N_2O from hydrologically connected terrestrial systems in the high

discharge period may have obscured relationships with NO_3-N. Previous studies in streams and rivers have also related external sources to N_2O supersaturation (Beaulieu et al. 2009; Turner et al. 2015).

Up-scaling and comparison with regional and global studies

The CO_2 and CH_4 fluxes measured in this study are within the range of those reported for 12 African sub-Saharan rivers, but the N_2O fluxes are threefold higher (Table 4). This may be due to the higher percentage of croplands in the Mara basin relative to the other river systems. Compared to other tropical and global studies, the mean daily CO_2 flux in the Mara (2832 mg C m^{-2} d^{-1}) was within the same order of magnitude as those reported for large Amazonian river basins (3373 and 6542 mg C m^{-2} d^{-1}) (Almeida et al. 2017; Sawakuchi et al. 2017), and for temperate river sites in the conterminous United States (3732 mg C m^{-2} d^{-1} (Butman and Raymond 2011). The range of CH_4 and N_2O fluxes in the Mara were within the global mean range reported by Stanley et al. (2016) (−125 – 5190 mg C m^{-2} d^{-1}) and Hu et al. (2016) (−588 – 178,556 µg N m^{-2} d^{-1}), respectively.

The basin-wide flux measurement of 5.92 Mg CO_2-C km^{-2} yr^{-1} for the Mara falls within the range of estimates reported for six river basins in sub-Saharan Africa (Borges et al. 2015) (1.24 – 47.64 Mg CO_2-C km^{-2} yr^{-1}; Table 4). The Borges et al. (2015) study was based on flux estimates mostly from higher-order streams (>> 10 m stream widths), while most of our observations (∼ 80%) were conducted at lower-order streams with < 10 m mean stream widths, which were clearly shown to dominate total catchment emissions (Fig. 5). For that reason, we would have expected much lower emissions per km^2 catchment area in the Borges et al. (2015) study (Table 4). One possible explanation is that the Mara Basin has a lower coverage of permanent headwater wetlands (< 0.08%) relative to the Congo, Betsiboka, Zambezi, and Tana basins in the Borges et al. (2015) study. Upstream wetlands may supply substantial amounts of dissolved CO_2 and CH_4 in streams and rivers during storm events (*see* Borges et al. 2019), which are then lost to the atmosphere through degassing in stream and river ecosystems. Another explanation is an overestimation of the stream width and subsequently stream surface area in the Borges et al. (2015) study, which was two times higher than our study (Table 4). The risk of overestimating stream surface area by using GIS approaches rather than in situ measurements has been previously shown in a temperate riverine catchment in the United States, where GIS based estimates of stream width of small-order streams were up to an order of magnitude higher than field measurements (Allen et al. 2018).

Our basin-wide flux estimate of 294 ± 35 Gg CO_2 eq yr^{-1} may be conservative, as we did not quantify emissions from permanent and seasonal wetlands within the catchment. The Mara basin has a relatively large permanent papyrus wetland at the mouth of the river, which covers ∼ 3% of the total basin

area. Borges et al. (2015) showed that Congo River wetlands alone doubled the contribution of greenhouse gas emissions from the entire sub-Saharan River network despite comprising only 1.5% of the basin, and hypothesized that wetlands are disproportionately important despite covering a relatively small catchment area. To estimate the possible contribution of the Mara Wetlands, we used previously measured CO_2 and CH_4 fluxes from a papyrus wetlands in Uganda (Were et al. 2021) and the Okavango delta in Botswana (Gondwe and Masamba 2014) to estimate annual emissions. These estimates ranged from 10 to 11 t CO_2 eq yr^{-1}, which is 35–40 times higher than our current basin estimate. This finding further highlights the importance of wetlands to basin scale flux estimates and the need to quantify emissions from them.

The upscaling sensitivity analysis showed a high sensitivity to discharge-width relationships due to their effect on stream area, and particularly because of the reactivity of the lower-order streams—that is, width increases with a small change in discharge compared to the larger-order rivers. This uncertainty was greater than using annual means for the measured greenhouse gas fluxes, suggesting that future efforts should focus on finer scale understanding of stream area under different seasonal conditions – especially in lower-order streams to allow better judgment of the importance of streams and rivers as regional and global sources of greenhouse gases. Our annual mean monthly ($\pm$ SD) discharge values of 11 ± 14.2 m^3 s^{-1} for the Nyangores (N1) and 9.3 ± 13 m^3 s^{-1} for the Amala (A1) represented a 30% and 130% increase in discharge, respectively, when compared to long-term (1950 – 2010) values (Nyangores; 8.44 m^3 s^{-1} and Amala; 4.01 m^3 s^{-1}) (McClain et al. 2014). This finding suggested that the year we sampled was a much wetter year compared to previous years. To quantify the uncertainties in our annual fluxes related to more wetter or drier years, we performed a sensitivity analysis on the response of the annual fluxes to a reduction of 25% in the number of high discharge days (i.e., from 120 to 90 d). The effect was that the annual emissions reduced by 18% to 241 Gg CO_2 eq yr^{-1}, an indicator that inter-annual emissions of the Mara basin may also vary substantially depending on more wetter or drier years.

Conclusions

This study measured seasonal fluxes of greenhouse gas emissions throughout a whole basin in the tropics and used discharge and associated changes in river width to upscale basin-wide greenhouse gas emissions. Based on warming potentials, low-order streams (1–3) contributed more than 80% of total basin-scale greenhouse gas emissions, and emissions during medium and high discharge periods were 10 times higher than in low discharge periods. Our approach of including width in our upscaling procedure proved important, and added 36% to the total estimate, showing that future research should aim to include changes in river surface area with

discharge, and consider longitudinal expansion, which was not included in this study. In high discharge periods, terrestrial inputs of greenhouse gases seem to dominate, with fluxes a function of both high k values and greater inputs from soils. The effect of land use/land cover was particularly evident in low-discharge seasons, when relationships with water quality variables (DO, DOC, and NO_3-N) and FBOM suggested in situ greenhouse gas production. Specifically, cropland sites had an order of magnitude higher N_2O emissions and 3 times higher CO_2 emissions than forest sites, while livestock sites had 3 times higher CH_4 emissions compared to the forest sites. Given that agricultural land use is a major factor increasing the source strengths of streams and rivers for greenhouse gases in the study region, increased conversion of forests and agricultural intensification has the possibility of increasing the contribution of the African continent to global atmospheric greenhouse gas sources. Future research should include the contribution of permanent and seasonal wetlands to basin-wide greenhouse gas emissions, which are likely an important but under-studied source of CH_4 in tropical river basins.

Data availability statement

All data and data analyses codes of this manuscript will be made available upon request to the corresponding author.

References

Abril, G., and others. 2014. Amazon River carbon dioxide outgassing fuelled by wetlands. Nature **505**: 395–398. doi:10.1038/nature12797

Aho, K. S., and P. A. Raymond. 2019. Differential response of greenhouse gas evasion to storms in forested and wetland streams. J. Geophys. Res. Biogeo. **124**: 649–662. doi:10.1029/2018JG004750

Allen, G. H., T. M. Pavelsky, E. A. Barefoot, M. P. Lamb, D. Butman, A. Tashie, and C. J. Gleason. 2018. Similarity of stream width distributions across headwater systems. Nat. Commun. **9**: 610. doi:10.1038/s41467-018-02991-w

Almeida, R. M., F. S. Pacheco, N. Barros, E. Rosi, and F. Roland. 2017. Extreme floods increase CO_2 outgassing from a large Amazonian river. Limnol. Oceanogr. **62**: 989–999. doi:10.1002/lno.10480

Audet, J., and others. 2019. Forest streams are important sources for nitrous oxide emissions. Glob. Chang. Biol. **26**: 629–641. doi:10.1111/gcb.14812

Battin, T. J., L. A. Kaplan, S. Findlay, C. S. Hopkinson, E. Marti, A. I. Packman, J. D. Newbold, and F. Sabater. 2008. Biophysical controls on organic carbon fluxes in fluvial networks. Nat. Geosci. **1**: 95–100. doi:10.1038/ngeo101

Baulch, H. M., P. J. Dillon, R. Maranger, and S. L. Schiff. 2011a. Diffusive and ebullitive transport of methane and nitrous oxide from streams: Are bubble-mediated fluxes important? J. Geophys. Res. Biogeo. **116**: G04028. doi:10.1029/2011JG001656

Baulch, H. M., S. L. Schiff, R. Maranger, and P. J. Dillon. 2011*b*. Nitrogen enrichment and the emission of nitrous oxide from streams. Global Biogeochem. Cycl. **25**: GB4013. doi:10.1029/2011GB004047

Beaulieu, J. J., C. P. Arango, and J. L. Tank. 2009. The effects of season and agriculture on nitrous oxide production in headwater streams. J. Environ. Qual. **38**: 637–646. doi:10.2134/jeq2008.0003

Bodmer, P., M. Heinz, M. Pusch, G. Singer, and K. Premke. 2016. Carbon dynamics and their link to dissolved organic matter quality across contrasting stream ecosystems. Sci. Total Environ. **553**: 574–586. doi:10.1016/j.scitotenv.2016.02.095

Bolleter, W. T., C. J. Bushman, and P. W. Tidwell. 1961. Spectrophotometric determination of ammonia as indophenol. Anal. Chem. **33**: 592–594. doi:10.1021/ac60172a034

Borges, A. V., and others. 2015. Globally significant greenhouse gas emissions from African inland waters. Nat. Geosci. **8**: 637–642. doi:10.1038/ngeo2486

Borges, A. V., and others. 2018. Effects of agricultural land use on fluvial carbon dioxide, methane and nitrous oxide concentrations in a large European river, the Meuse (Belgium). Sci. Total Environ. **610–611**: 342–355. doi:10.1016/j.scitotenv.2017.08.047

Borges, A. V., and others. 2019. Variations in dissolved greenhouse gases (CO_2, CH_4, N_2O) in the Congo river network overwhelmingly driven by fluvial-wetland connectivity. Biogeosciences **16**: 3801–3834. doi:10.5194/bg-16-3801-2019

Butman, D., and P. A. Raymond. 2011. Significant efflux of carbon dioxide from streams and rivers in the United States. Nat. Geosci. **4**: 839–842. doi:10.1038/ngeo1294

de Angelis, M. A., and M. I. Scranton. 1993. Fate of methane in the Hudson river and estuary. Global Biogeochem. Cycl. **7**: 509–523. doi:10.1029/93GB01636

Drake, T. W., P. A. Raymond, and R. G. Spencer. 2018. Terrestrial carbon inputs to inland waters: A current synthesis of estimates and uncertainty. Limnol. Oceanogr. Lett. **3**: 132–142.

Drake, T. W., and others. 2019. Mobilization of aged and biolabile soil carbon by tropical deforestation. Nat. Geosci. **12**: 541–546. doi:10.1038/s41561-019-0384-9

Duc, N. T., P. Crill, and D. Bastviken. 2010. Implications of temperature and sediment characteristics on methane formation and oxidation in lake sediments. Biogeochemistry **100**: 185–196. doi:10.1007/s10533-010-9415-8

Dutton, C. L., and others. 2019. A 2000-year sediment record reveals rapidly changing sedimentation and land use since the 1960s in the Upper Mara-Serengeti ecosystem. Sci. Total Environ. **664**: 148–160. doi:10.1016/j.scitotenv.2019.01.421

Duvert, C., and others. 2020. Net landscape carbon balance of a tropical savanna: Relative importance of fire and aquatic export in offsetting terrestrial production. Glob. Chang. Biol. **26**: 5899–5913. doi:10.1111/gcb.15287

Gondwe, M. J., and W. R. Masamba. 2014. Spatial and temporal dynamics of diffusive methane emissions in the Okavango Delta, northern Botswana, Africa. Wetlands Ecol. Manage. **22**: 63–78. doi:10.1007/s11273-013-9323-5

Gore, J. A. 2007. Discharge measurements and streamflow analysis, p. 51–77. *In* F. R. Hauer and G. A. Lamberti [eds.], Methods in stream ecology, 2nd ed.., chap. 3. Academic Press. doi:10.1016/B978-012332908-0.50005-X

Hotchkiss, E. R., R. O. Hall Jr., R. A. Sponseller, D. Butman, J. Klaminder, H. Laudon, M. Rosvall, and J. Karlsson. 2015. Sources of and processes controlling CO_2 emissions change with the size of streams and rivers. Nat. Geosci. **8**: 696–699. doi:10.1038/ngeo2507

Hu, M., D. Chen, and R. A. Dahlgren. 2016. Modeling nitrous oxide emission from rivers: A global assessment. Glob. Chang. Biol. **22**: 3566–3582. doi:10.1111/gcb.13351

Intergovernmental Panel on Climate Change. 2014. Climate change 2013—The physical science basis: Working group I contribution to the fifth assessment report of the Intergovernmental Panel on Climate Change. Cambridge Univ. Press. doi:10.1017/CBO9781107415324

Johnson, M. S., J. Lehmann, S. J. Riha, A. V. Krusche, J. E. Richey, J. P. H. Ometto, and E. G. Couto. 2008. CO_2 efflux from Amazonian headwater streams represents a significant fate for deep soil respiration. Geophys. Res. Lett. **35**: L17401. doi:10.1029/2008GL034619

Knowles, R. 1982. Denitrification. Microbiol. Rev. **46**: 43–70. doi:10.1128/CMR.5.4.356.Updated

Koné, Y. J. M., G. Abril, B. Delille, and A. V. Borges. 2010. Seasonal variability of methane in the rivers and lagoons of Ivory Coast (West Africa). Biogeochemistry **100**: 21–37. doi:10.1007/s10533-009-9402-0

Koschorreck, M., Y. T. Prairie, J. Kim, and R. Marcé. 2021. CO_2 is not like CH_4–limits of and corrections to the headspace method to analyse pCO_2 in fresh water. Biogeosciences **18**: 1619–1627. doi:10.5194/bg-18-1619-2021

Lambert, T., S. Bouillon, F. Darchambeau, C. Morana, F. A. E. Roland, J. Descy, and A. V. Borges. 2017. Effects of human land use on the terrestrial and aquatic sources of fluvial organic matter in a temperate river basin (The Meuse River, Belgium). Biogeochemistry **136**: 191–211. doi:10.1007/s10533-017-0387-9

Liu, S., and P. A. Raymond. 2018. Hydrologic controls on pCO_2 and CO_2 efflux in US streams and rivers. Limnol. Oceanogr. Lett. **3**: 428–435. doi:10.1002/lol2.10095

Lupon, A., B. A. Denfeld, H. Laudon, J. Leach, J. Karlsson, and R. A. Sponseller. 2019. Groundwater inflows control patterns and sources of greenhouse gas emissions from streams. Limnol. Oceanogr. **64**: 1545–1557. doi:10.1002/lno.11134

Marwick, T. R., F. Tamooh, B. Ogwoka, C. Teodoru, A. V. Borges, F. Darchambeau, and S. Bouillon. 2014. Dynamic

seasonal nitrogen cycling in response to anthropogenic N loading in a tropical catchment, Athi-Galana-Sabaki River, Kenya. Biogeosciences **11**: 443–460. doi:10.5194/bg-11-443-2014

Marzadri, A., M. M. Dee, D. Tonina, A. Bellin, and J. L. Tank. 2017. Role of surface and subsurface processes in scaling N_2O emissions along riverine networks. Proc. Natl. Acad. Sci. **114**: 4330–4335. doi:10.1073/pnas.1617454114

Marzadri, A., G. Amatulli, D. Tonina, A. Bellin, L. Q. Shen, G. H. Allen, and P. A. Raymond. 2021. Global riverine nitrous oxide emissions: The role of small streams and large rivers. Sci. Total Environ. **776**: 145148. doi:10.1016/j.scitotenv.2021.145148

Masese, F. O., J. S. Salcedo-Borda, G. M. Gettel, K. Irvine, and M. E. McClain. 2017. Influence of catchment land use and seasonality on dissolved organic matter composition and ecosystem metabolism in headwater streams of a Kenyan river. Biogeochemistry **132**: 1–22. doi:10.1007/s10533-016-0269-6

Mati, B. M., S. Mutie, H. Gadain, P. Home, and F. Mtalo. 2008. Impacts of land-use/cover changes on the hydrology of the transboundary Mara River, Kenya/Tanzania. Lakes Reserv. Res. Manage. **13**: 169–177. doi:10.1111/j.1440-1770.2008.00367.x

McClain, M. E., and others. 2014. Comparing flow regime, channel hydraulics, and biological communities to infer flow–ecology relationships in the Mara River of Kenya and Tanzania. Hydrol. Sci. J. **59**: 801–819. doi:10.1080/02626667.2013.853121

Mwanake, R. M., G. M. Gettel, K. S. Aho, D. W. Namwaya, F. O. Masese, K. Butterbach-Bahl, and P. A. Raymond. 2019. Land use, not stream order, controls N_2O concentration and flux in the upper Mara River basin, Kenya. J. Geophys. Res. Biogeo. **124**: 3491–3506. doi:10.1029/2019jg005063

Patton, C. J., and J. R. Kryskalla. 2011. Colorimetric determination of nitrate plus nitrite in water by enzymatic reduction, automated discrete analyzer methods. U.S. Geological Survey Techniques and Methods, Book 5, p. 34. doi:10.3133/tm5B8

Quick, A. M., W. J. Reeder, T. B. Farrell, D. Tonina, K. P. Feris, and S. G. Benner. 2019. Nitrous oxide from streams and rivers: A review of primary biogeochemical pathways and environmental variables. Earth Sci. Rev. **191**: 224–262. doi:10.1016/j.earscirev.2019.02.021

Rasera, M. F. L., A. V. Krusche, J. E. Richey, M. V. R. Ballester, and R. L. Victória. 2013. Spatial and temporal variability of pCO_2 and CO_2 efflux in seven Amazonian rivers. Biogeochemistry **116**: 241–259. doi:10.1007/s10533-013-9854-0

Raymond, P. A., N. F. Caraco, and J. J. Cole. 1997. Carbon dioxide concentration and atmospheric flux in the Hudson river. Estuaries **20**: 381–390. doi:10.2307/1352351

Raymond, P. A., and J. J. Cole. 2001. Gas exchange in rivers and estuaries: Choosing a gas transfer velocity. Estuaries **24**: 312–317. doi:10.2307/1352954

Raymond, P. A., and J. E. Saiers. 2010. Event controlled DOC export from forested watersheds. Biogeochemistry **100**: 197–209. doi:10.1007/s10533-010-9416-7

Raymond, P. A., C. J. Zappa, D. Butman, T. L. Bott, J. Potter, P. Mulholland, A. E. Laursen, W. H. McDowell, and D. Newbold. 2012. Scaling the gas transfer velocity and hydraulic geometry in streams and small rivers. Limnol. Oceanogr. **2**: 41–53. doi:10.1215/21573689-1597669

Raymond, P. A., and others. 2013. Global carbon dioxide emissions from inland waters. Nature **503**: 355–359. doi:10.1038/nature12760

Raymond, P. A., J. E. Saiers, and W. V. Sobczak. 2016. Hydrological and biogeochemical controls on watershed dissolved organic matter transport: Pulse-shunt concept. Ecology **97**: 5–16. doi:10.1890/14-1684.1

Richey, J. E., A. H. Devol, S. C. Wofsy, R. Victoria, and M. N. G. Riberio. 1988. Biogenic gases and the oxidation and reduction of carbon in Amazon river and floodplain waters. Limnol. Oceanogr. **33**: 551–561. doi:10.4319/lo.1988.33.4.0551

Rocher-Ros, G., R. A. Sponseller, W. Lidberg, C. M. Mörth, and R. Giesler. 2019. Landscape process domains drive patterns of CO_2 evasion from river networks. Limnol. Oceanogr. Lett. **4**: 87–95. doi:10.1002/lol2.10108

Rosentreter, J. A., and others. 2021. Half of global methane emissions come from highly variable aquatic ecosystem sources. Nat. Geosci. **14**: 225–230. doi:10.1038/s41561-021-00715-2

Sawakuchi, H. O., D. Bastviken, A. O. Sawakuchi, A. V. Krusche, M. V. R. Ballester, and J. E. Richey. 2014. Methane emissions from Amazonian rivers and their contribution to the global methane budget. Glob. Chang. Biol. **20**: 2829–2840. doi:10.1111/gcb.12646

Sawakuchi, H. O., and others. 2017. Carbon dioxide emissions along the lower Amazon river. Front. Mar. Sci. **4**: 1–12. doi:10.3389/fmars.2017.00076

Schade, J. D., J. Bailio, and W. H. McDowell. 2016. Greenhouse gas flux from headwater streams in New Hampshire, USA: Patterns and drivers. Limnol. Oceanogr. **61**: 165–174. doi:10.1002/lno.10337

Schumacher, B. A. 2002. Methods for the determination of total organic carbon (TOC) in soils and sediments. U.S. Environmental Protection Agency. EPA/600/R-02/069 (NTIS PB2003-100822).

Shelley, F., J. Grey, and M. Trimmer. 2014. Widespread methanotrophic primary production in lowland chalk rivers. Proc. Roy. Soc. B Biol. Sci. **281**: 1783. doi:10.1098/rspb.2013.2854

Stanley, E. H., N. J. Casson, S. T. Christel, J. T. Crawford, L. C. Loken, and S. K. Oliver. 2016. The ecology of methane in streams and rivers: Patterns, controls, and global significance. Ecol. Monogr. **86**: 146–171. doi:10.1890/15-1027

Strahler, A. N. 1952. Hypsometric (area-altitude) analysis of erosional topography. GSA Bull. **63**: 1117–1142. doi:10.1130/0016-7606(1952)63[1117:HAAOET]2.0.CO;2

Teodoru, C. R., F. C. Nyoni, A. V. Borges, F. Darchambeau, I. Nyambe, and S. Bouillon. 2015. Dynamics of greenhouse gases (CO_2, CH_4, N_2O) along the Zambezi river and major tributaries, and their importance in the riverine carbon budget. Biogeosciences **12**: 2431–2453. doi:10.5194/bg-12-2431-2015

Turner, P. A., T. J. Griffis, X. Lee, J. M. Baker, R. T. Venterea, and J. D. Wood. 2015. Indirect nitrous oxide emissions from streams within the US Corn Belt scale with stream order. Proc. Natl. Acad. Sci. **112**: 9839–9843. doi:10.1073/pnas.1503598112

Wallin, M. B., and others. 2018. Carbon dioxide and methane emissions of Swedish low-order streams—A national estimate and lessons learnt from more than a decade of observations. Limnol. Oceanogr. **3**: 156–167. doi:10.1002/lol2.10061

Wallin, M. B., J. Audet, M. Peacock, E. Sahlée, and M. Winterdahl. 2020. Carbon dioxide dynamics in an agricultural headwater stream driven by hydrology and primary production. Biogeosciences **17**: 2487–2498. doi:10.5194/bg-17-2487-2020

Wanyama, I., D. E. Pelster, C. Arias-Navarro, K. Butterbach-Bahl, L. V. Verchot, and M. C. Rufino. 2018. Management intensity controls soil N_2O fluxes in an Afromontane ecosystem. Sci. Total Environ. **624**: 769–780. doi:10.1016/j.scitotenv.2017.12.081

Weiss, R. F. 1974. Carbon dioxide in water and seawater: The solubility of a non-ideal gas. Mar. Chem. **2**: 203–215. doi:10.1016/0304-4203(74)90015-2

Weiss, R. F., and B. A. Price. 1980. Nitrous oxide solubility in water and seawater. Mar. Chem. **8**: 347–359. doi:10.1016/0304-4203(80)90024-9

Were, D., F. Kansiime, T. Fetahi, and T. Hein. 2021. Carbon dioxide and methane fluxes from various vegetation communities of a natural tropical freshwater wetland in different seasons. Environ. Process. **8**: 553–571. doi:10.1007/s40710-021-00497-0

Wiesenburg, D. A., and N. L. Guinasso. 1979. Equilibrium solubilities of methane, carbon monoxide, and hydrogen in water and sea water. J. Chem. Eng. Data **24**: 356–360. doi:10.1021/je60083a006

Winkler, K., R. Fuchs, M. Rounsevell, and M. Herold. 2021. Global land use changes are four times greater than previously estimated. Nat. Commun. **12**: 1–10. doi:10.1038/s41467-021-22702-2

Yao, G., Q. Gao, Z. Wang, X. Huang, T. He, Y. Zhang, S. Jiao, and J. Ding. 2007. Dynamics of CO_2 partial pressure and CO_2 outgassing in the lower reaches of the Xijiang river, a subtropical monsoon river in China. Sci. Total Environ. **376**: 255–266. doi:10.1016/j.scitotenv.2007.01.080

Yao, Y., H. Tian, H. Shi, S. Pan, R. Xu, N. Pan, and J. G. Canadell. 2020. Increased global nitrous oxide emissions from streams and rivers in the Anthropocene. Nat.Clim. Change **10**: 138–142. doi:10.1038/s41558-019-0665-8

Zhang, L., X. Xia, S. Liu, S. Zhang, S. Li, J. Wang, and Raymond, P. A. (2020). Significant methane ebullition from alpine permafrost rivers on the East Qinghai-Tibet Plateau. Nature Geoscience, **13**: 349–354. https://doi.org/10.1038/s41561-020-0571-8

Zuur, A. F., E. N. Ieno, and G. M. Smith. 2007. Analysing ecological data. Springer, p. 680. doi:10.1007/978-0-387-45972-1

Conflict of Interest.

None declared.

Submitted 26 April 2021
Revised 06 December 2021
Accepted 10 May 2022

Associate editor: Robert O. Hall Jr.